Analysis of the Photoluminescence Bandgap Temperature Dependence to Investigate the Doping of Micrometric Size GaAs Crystals Grown on Silicon for Tandem Solar Cells Applications

Denis Mencaraglia, Alexandre Jaffré, Guillaume Chau, J Alvarez, James Patrick Connolly, Laurie Dentz, Géraldine Hallais, Charles Renard

physica status solidi pss a
www.pss-a.com

Analysis of the Photoluminescence Bandgap Temperature Dependence to Investigate the Doping of Micrometric Size GaAs Crystals Grown on Silicon for Tandem Solar Cells Applications

Denis Mencaraglia, Alexandre Jaffré, Guillaume Chau, Jose Alvarez, James Patrick Connolly, Laurie Dentz, Geraldine Hallais, and Charles Renard*

This work presents and discusses the extraction of the active dopants density of GaAs layers from the modeling of the bandgap temperature dependence derived from photoluminescence measurements.

1. Introduction

The final goal of this work is to extract the active dopant density of micrometric size GaAs crystals grown on silicon for the further optimization of III–V on silicon multijunction solar cells. The integration of these crystals in a regular way to have a quasicomplete covering of the Si substrate, without coalescence of the GaAs microcrystals to maintain their very good electronic properties, would be very useful to develop III–V/Si tandem cells. High-efficiency III–V/Ge multijunction solar cells are well developed already for space applications. However, in order to bring this design to photovoltaic terrestrial applications, it would be very advantageous to replace the costly Ge substrate with Si. Effectively, according to a realistic model, we have shown that in a first instance a GaAs/Si tandem cell could achieve an efficiency of 29.2% under AM1.5G spectrum.[1] This would also open the route for low-cost, high-efficiency triple junctions.

A first important challenge is the growth of a lattice-mismatched material without dislocations nor antiphase domains. Using chemical beam epitaxial lateral overgrowth (CBE ELO) on tunnel oxide from nanoseeds with the metalorganic precursors trimethylgallium (TMGa) and tertiary-butylarsine (TBAs), we were able to grow such good quality micrometer size GaAs crystals on silicon.[2] To further develop a GaAs/Si tandem cell, the doping of these GaAs crystals has now to be accurately controlled. The residual doping control in a single GaAs microcrystal is then a prerequisite first step to developing future design and technology of multijunction solar cells based on this approach. Local-scale electrical $I(V)$ measurements of the GaAs/Si heterojunction performed with conducting probe atomic force microscopy have demonstrated a high rectification ratio.[2] However, a high p-type nonintentional doping level was indicated, the origin of which will be further discussed in the Section 4. The precise doping level determination in a single μ-crystal by local $I(V)$ or $C(V)$ measurements is difficult because in the first case the estimation is too indirect and in the latter one the capacitance values are too small to be easily measured. To obtain a better estimation of the doping level, we have developed a contactless method based on the measurement of the variation of the bandgap versus temperature derived from photoluminescence (PL) measurements.[3] In this past preliminary work, we used Varshni's semiempirical relation which has been used for many years to describe semiconductors bandgap dependence with temperature.[4] In the present work, we follow Pässler's approach[5] who has shown the inadequate analytical structure of Varshni's formula and proposed an analytical four-parameters expression providing better agreement with data and better estimations of physical parameters. We used this last approach while also taking into account the bandgap narrowing (BGN) in our substantially p-doped materials. As PL measurements can also be affected by the different sizes of our GaAs crystals in the submicrometric range, we want here first to assess the method on full-plate GaAs layers homoepitaxially grown on GaAs wafers, the crystal orientation of which was carefully chosen to mimic the heteroepitaxial growth on silicon. The application of our method will be illustrated with the investigation of the influence on the residual doping of the V/III precursors ratio in the vapor phase.

D. Mencaraglia, A. Jaffré, G. Chau, J. Alvarez, J. P. Connolly
GeePs
Group of Electrical Engineering Paris
CNRS
CentraleSupelec
Université Paris-Saclay
Sorbonne Université
11 rue Joliot-Curie, Plateau de Moulon, 91192 Gif-sur-Yvette, France
E-mail: denis.mencaraglia@centralesupelec.fr

L. Dentz, G. Hallais, C. Renard
C2N
Centre de Nanosciences et de Nanotechnologies
CNRS
Université Paris-Saclay
10 Bd Thomas Gobert, 91120 Palaiseau, France

The ORCID identification number(s) for the author(s) of this article can be found under https://doi.org/10.1002/pssa.202400609.

DOI: 10.1002/pssa.202400609

The content of this article is organized as follows: Section 2 presents the modeling method to describe the bandgap temperature dependence, Section 3 gives the experimental details and the results are shown and discussed in Section 4 before to conclude on the pros and cons of the method in Section 5 giving also some perspectives for future work.

2. Modeling of the Bandgap Temperature Dependence

The proposed analytical four-parameters expression introduced by Pässler to model the bandgap variation with temperature is written as[5]

$$E_g(T) = E_g(0) - \frac{\alpha\theta_p}{2}\left[\sqrt[p]{1+\left(\frac{2T}{\theta_p}\right)^p} - 1\right] \quad (1)$$

where T is the sample lattice temperature; α representing the limiting magnitude of the slope of the $E_g(T \to \infty)$curve, θ_p being approximately the average phonon temperature, and p being linked to the material-specific degree of phonon dispersion.

The four-parameter Pässler's dataset determined by fitting the high precision PL data of Grilli et al.[6] measured on a high-quality nominally undoped GaAs sample grown by molecular beam epitaxy is $E_g(0) = 1.519$ eV, $p = 2.44$, $\alpha = 0.472 \times 10^{-3}$ eV K^{-1}, $\theta_p = 230$ K. Note that throughout this article, numerical values of these parameters will be expressed with these same units and that these units may sometimes appear omitted inside the figures.

The bandgap narrowing $\Delta E_{BGN} = [E_g(0)]_{Intrinsic} - [E_g(0)]_{Doped}$ due to p-type doping is modeled with the Jain et al. expression[7,8]

$$\Delta E_{BGN} = E_{gi}(0) - E_{gd}(0) = AP^{\frac{1}{3}} + BP^{\frac{1}{4}} + CP^{\frac{1}{2}} \quad (2)$$

where P is the hole or acceptor concentration (full ionization assumed). A, B, and C are the coefficients of the BGN due to majority–majority carrier exchange, minority–majority correlation, and carrier–ion interaction, respectively. From their theoretical expressions obtained using a low temperature approximation, Jain et al. calculated the following numerical values of these coefficients for p-doped GaAs:[7,8] $A = 9.83 \times 10^{-9}$ eV cm, $B = 3.90 \times 10^{-7}$ eV cm$^{3/4}$, $C = 3.90 \times 10^{-12}$ eV cm$^{3/2}$. Note that these numerical values are dependent of the type of doping but do not depend on the doping density itself, at least in the medium or high doping range where Jain et al. assumptions are valid.

We express now Equation (1) for a doped material by inserting explicitly the letter "*d*" in the subscripts

$$E_{gd}(T) = E_{gd}(0) - \frac{\alpha\theta_p}{2}\left[\sqrt[p]{1+\left(\frac{2T}{\theta_p}\right)^p} - 1\right] \quad (3)$$

on the understanding that the parameters p, α, θ_p may also be doping dependent with different numerical values from the intrinsic case given above just after Equation (1). Replacing $E_{gd}(0)$ in Equation (3) with its expression derived from Equation (2), we get

$$E_{gd}(T) = E_{gi}(0) - \left(AP^{\frac{1}{3}} + BP^{\frac{1}{4}} + CP^{\frac{1}{2}}\right) - \frac{\alpha\theta_p}{2}\left[\sqrt[p]{1+\left(\frac{2T}{\theta_p}\right)^p} - 1\right] \quad (4)$$

The experimental bandgap variation with temperature can be adjusted in two equivalent ways, either with Equation (3) or (4). Using Equation (3) will lead directly to $E_{gd}(0)$ and then to the BGN $\Delta E_{BGN} = E_{gi}(0) - E_{gd}(0)$, whereas with Equation (4) we will get directly the active dopant concentration P. In both cases, four adjustable parameters will be needed, the three of which being common to Equation (3) and (4), with naturally identical extracted values as these two equations describe the temperature dependence in the same way. A least-squares fit of Equation (3) or (4) to the experimental bandgap variation with temperature has been made with a commercial data analysis application using the Levenberg–Marquardt algorithm.

3. Experimental Section

3.1. Investigated Samples

3.1.1. Bulk Reference Wafers

To test our method in a large range of carrier density, we use two GaAs bulk reference wafers, one p(Zn)-GaAs wafer being p-type doped with a Zn concentration comprised between 2×10^{18} and 5×10^{19} cm^{-3} as indicated by the fabricant and a semi-insulating (S-I) (110) GaAs wafer nominally undoped with a resistivity and carrier mobility around 2×10^8 ohm cm^{-1} and 5×10^3 cm^2 V^{-1} s^{-1} respectively. For this high-resistivity wafer, these parameters are consistent with a carrier (electron) density of 6×10^6 cm^{-3}.

3.1.2. Gaas Epitaxial Layers

As we mentioned earlier in the Introduction, PL measurements can also be affected by the different sizes of our GaAs crystals in the submicrometric range when they are grown on silicon using CBE ELO on tunnel oxide from nanoseeds. So our purpose here is first to assess the method on full-plate GaAs layers homoepitaxially grown on GaAs wafers, the crystal orientation of which was carefully chosen to mimic the heteroepitaxial growth on silicon. Generally, the (001) surface is the reference surface for GaAs homoepitaxy. However, we observed during heteroepitaxies of GaAs on Si that the lateral growth took place following the [110] direction.[9] Thus, in order to remain within an equivalent doping mechanism, we have chosen to carry out GaAs homoepitaxies on GaAs (110) substrates. Indeed, the major difference between the (001) surface and the (110) surface is the number of bonds between the Ga and As atoms on the surface. On a (001) surface, an As atom is linked to two Ga atoms. But on a (110) surface, an As atom is only bonded to a single Ga atom. It follows that an As atom is more strongly bound on a (001) surface (terminated by a monolayer of Ga) than on a (110) surface. This leads to easier desorption of As atoms on a (110) surface and therefore lower As incorporation for growth.[10] This lower quantity of As atoms available for growth has a direct

consequence on the doping of epitaxial GaAs. Thus, as the doping of the epitaxial layer strongly depends on the orientation of the GaAs substrate, we therefore chose to carry out homoepitaxies on GaAs(110) in order to be close to the doping mechanisms of our heteroepitaxies on Si.

The epitaxial growth was carried out in a chemical beam epitaxy system with a base pressure of 2×10^{-8} Pa. TMGa and TBAs were used as gas sources. The epi-ready (110) N(Si)-GaAs wafers ($0.8 \times 10^{18} - 4.0 \times 10^{18}$ cm^{-3}) were slowly annealed in situ up to 400 °C, the pressure being maintained below 3×10^{-6} Pa. Then, at 410 °C the GaAs substrates were exposed under a TBAs total pressure of 1.32 Pa and ramped up to 620 °C for deoxidation. The substrate temperature is then lowered under TBAs at 550 °C for GaAs epitaxy. TMGa was then also introduced and the total pressure was increased up to 6.6 Pa achieving a V/III ratio R=[TBAs]/[TMGa] in the range of 6–14, while the temperature was kept at 550 °C for a growth duration around 40 min achieving a layer thickness around 300 nm. These growth parameters are summarized in **Table 1**.

Table 1. Growth parameters of the investigated homoepitaxial GaAs layers under different V/III ratio and a total pressure of 6.6 Pa during 40 nm after a nucleation step at 410 °C under TBAs only. The layer thickness is around 300 nm.

Homoepitaxial layers	Growth temperature [°C]	[TBAs]/[TMGa]
GaAs#299	550	6
GaAs#304	550	8
GaAs#300	550	10
GaAs#301	550	12
GaAs#302	550	14

3.2. PL Measurements

PL measurements were performed on a WITec alpha-300R confocal microscope in a backscattering configuration. Samples were under vacuum at 10^{-1} Pa in a Linkam Thermal stage and probed at a requested temperature imposed by the temperature controller from 80 to 340 K, each 20 K. Samples were excited at 532 nm through an Olympus 20x long working distance objective, with 30 μW laser power (1.5 μW μm^{-2}). This injection power is high but we verified that it does not affect the PL maximum peak. For μ-PL analysis, we use a 200 μm core diameter fiber, a Princeton SP-2300 spectrometer with a 150 grooves mm^{-1} grating and a Si CCD camera, cooled down to −70 °C via a three-stage Peltier cooler.

For PL measurements at each temperature step, we proceed as follows: we first reach 80 K, and then heat up the sample to 340 K by taking spectra each 20 K. For the first step, we wait for 30 min at 80 K to let the sample thermalize before recording a spectrum. Then for each next step we wait for 10 min.

4. Results and Discussion

4.1. Analysis of the Bandgap Variation with Temperature for the p(Zn)-GaAs Reference Wafer

We present first the parameters extraction method applied to the p(Zn)-GaAs reference wafer. Examples of its PL spectra are presented in **Figure 1**a for 14 temperatures in the range [80 K, 340 K].

The main peak is attributed to a combination of excitonic and band-to-band transitions with an energetic position of the PL maximum close to the $n = 1$ exciton state.[6] In a practical

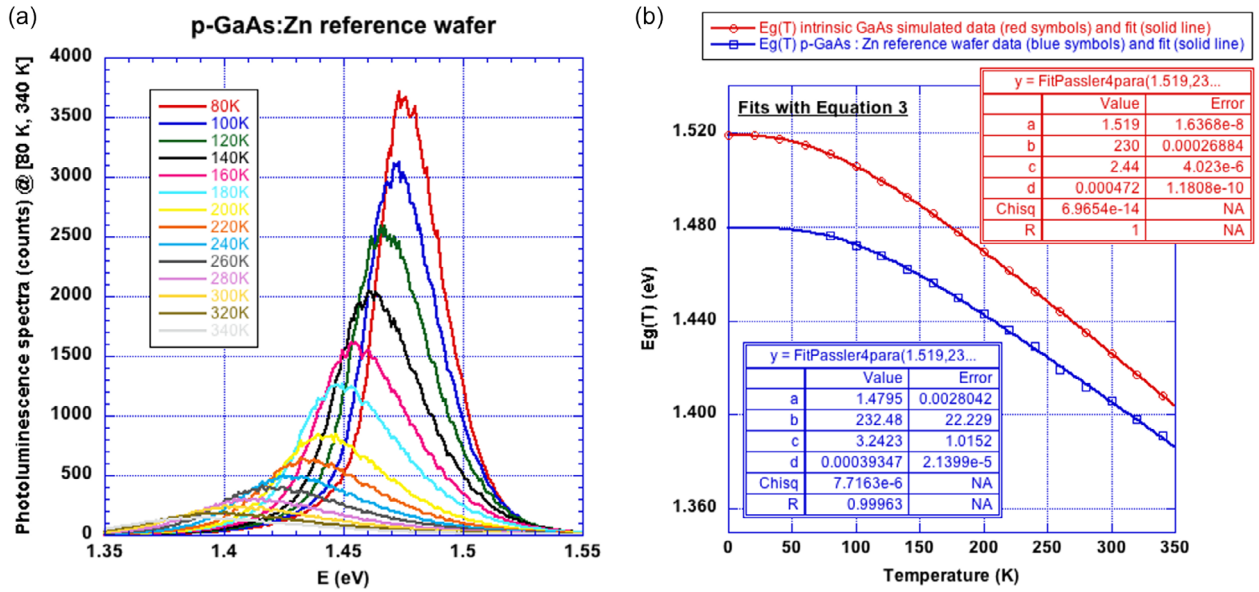

Figure 1. Analysis of the bandgap variation with temperature of the p(Zn)-GaAs reference wafer: a) PL spectra at different temperatures in the range [80 K, 340 K] with 20 K steps and b) (blue symbols) variations with T of the PL peak maximum data derived from (a) fitted using Equation (3) (blue line) with the values of the parameters a, b, c, and d (standing for $E_{gd}(0)$, θ_p, p, and α, respectively) given in the blue insert. For comparison, in red color are shown the same elements for a high-quality nominally undoped GaAs material modeled with the four-parameter Pässler's dataset determined by fitting the high precision PL data of Grilli et al.[6] (already referred to below Equation (1)).

way, at each temperature T we assimilate the fundamental gap $E_g(T)$ to this maximum because on one hand the exciton binding energy is small, around 4 meV, and on the other hand nearly constant over the temperature range investigated here, its variation being of the order of the experimental uncertainty around a few tenths of meV. If greater accuracy were required, the value of the exciton binding energy could be evaluated at each temperature as was done by Grilli et al.[6] and added to the peak position.

4.1.1. Curve Fitting with Equation (3)

In this way from Figure 1a, we then determine the experimental bandgap variation versus the temperature shown in Figure 1b (blue symbols) for the p(Zn)-GaAs wafer. The corresponding fitted curve with Equation (3) is represented by the blue line and the extracted parameters with their uncertainties are shown in the blue insert. The letters *a*, *b*, *c*, and *d*, respectively, refer to the four parameters $E_{gd}(0)$, θ_p, p, and α of Equation (3). For comparison with an undoped GaAs material, we have presented in red color its bandgap variation calculated with the four-parameter Pässler's dataset determined by fitting the high precision PL data of Grilli et al.[6] (already referred to below Equation (1)). As we can see in the red insert, the numerical values of the four parameters are well recovered with the curve fitting procedure with very low absolute uncertainties indicated in the last column of the insert. From this comparison with an undoped GaAs material we can note the lower value of the bandgap at each temperature for the p-doped GaAs reference wafer, as is expected from the bandgap narrowing effect. In particular, the extracted values of the bandgap at $T = 0$ are 1.4795 and 1.519 eV, respectively, from which we can calculate for the p(Zn)-GaAs reference wafer a BGN value $\Delta E_{BGN} = E_{gi}(0) - E_{gd}(0)$ equal to 0.0395 eV.

4.1.2. Curve Fitting with Equation (4)

In the same way as was done in the preceding paragraph, we now proceed with Equation (4) instead of Equation (3) for the curve fitting procedure. As we can see from the comparison of these two equations, three fitting parameters (θ_p, p, and α) are common among the four ones, and fitting now with Equation (4), we will get the concentration P instead of getting $E_{gd}(0)$ from the fit with Equation (3). These two parameters are linked obviously by Equation (2) and the extracted numerical values of the three common parameters should be the same for the two fits with either Equation (3) or (4) applied to the same data. Naturally, this will be verified experimentally but the interest of fitting either with Equation (3) or (4) is that we will also know the uncertainties on the extracted parameters so that it will be possible to check the precision of the bandgap narrowing modeling with Equation (2).

Figure 2a presents exactly the same experimental data as in Figure 1b and the lines are the corresponding fitted curves with the numerical values of the parameters indicated in the inserts.

The parameter "*a*" now stands for the doping density P of Equation (4), the rounded extracted numerical value of which is equal to $3.6 \times 10^{18} \pm 0.8 \times 10^{18}$ cm^{-3} well inside the fabricant specifications range of 2×10^{18} to 5×10^{19} cm^{-3}. Note also the very low extracted doping density value (between 5.4×10^{11} and 1.6×10^{12} cm^{-3}) corresponding to an undoped GaAs material

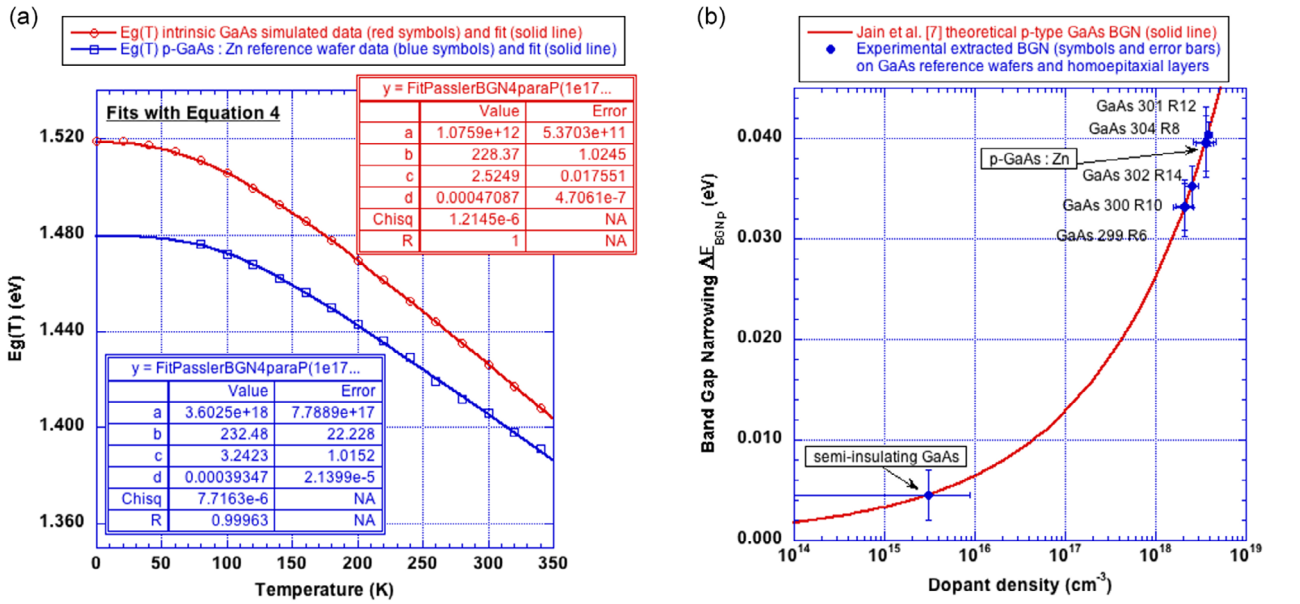

Figure 2. a) Analysis of the bandgap variation with temperature of the p(Zn)-GaAs reference wafer (blue symbols) fitted using Equation (4) (blue line) with the values of the parameters *a*, *b*, *c*, and *d* (standing for P, θ_p, p, and α, respectively) given in the blue insert. For comparison, in red color are shown the same elements for a high-quality nominally undoped GaAs material modeled with the four-parameter Pässler's dataset determined by fitting the high precision PL data of Grilli et al.[6] (already referred to below Equation (1)); b) representative curve (solid line) of the theoretical BGN law expressed by Equation (2) versus the concentration P and experimental data points (blue symbols) corresponding to the two GaAs reference wafers and to the GaAs homoepitaxial layers which are discussed in Section 4.2.

represented in red color in Figure 2a, even if its precise value is not significant, the important point being that it is well below practical doping densities in GaAs. This value around $10^{12}\,cm^{-3}$ gives a first indication of the lowest limit of doping density to which the method could be sensitive, at least for a nominally undoped "theoretical" GaAs material, the data of which are constructed with Equation (1) and the four-parameter Pässler's dataset and then fitted with Equation (4).

To have a more realistic indication of the method sensitivity on the doping or carrier density extraction, we applied the curve fitting with both Equation (3) and (4) to a real sample, the semi-insulating GaAs wafer described in Section 3.1.1. We found $E_{gd}(0) = 1.5145 \pm 0.0025$ eV leading to a BGN value $\Delta E_{BGN} = E_{gi}(0) - E_{gd}(0) = 0.0045 \pm 0.0025$ eV and a concentration P between 10^{14} and $10^{16}\,cm^{-3}$. The uncertainties of the extracted values are large in this range as it can be easily realized with Figure 2b where are presented both the theoretical BGN law expressed by Equation (2) (solid line) versus the concentration P and experimental data points. For the lowest densities less than $10^{16}\,cm^{-3}$ we can see that on one hand the predicted variation of the BGN versus the density is weak and on the other hand the experimental BGN contribution decreases when the carrier density decreases, leading to higher experimental uncertainties. We deduce then that this doping content extraction method is sensitive for densities higher than $10^{16}\,cm^{-3}$. We have also reported in Figure 2b the data corresponding to the p(Zn)-GaAs reference wafer located close to the highest part of the curve. The other data points are related to the GaAs homoepitaxial layers and are presented now in the next section.

4.2. Analysis of the Bandgap Variation with Temperature for the GaAs Homoepitaxial Layers

4.2.1. Curve Fitting with Both Equation (3) and (4)

The same method as the one described previously in Section 4.1 for the GaAs reference wafers has been applied to the homoepitaxial GaAs layers grown with different V/III ratio R = [TBAs]/[TMGa] in the range of 6–14. The results are summarized in **Table 2** and reported in Figure 2b.

Table 2. Numerical values of the bandgap narrowing and the doping density extracted from the curve fitting with respectively Equation (3) or (4) to the experimental bandgap variation with temperature of the homoepitaxial layers grown with different R = V/III ratio, the other growth parameters being identical. The given uncertainties on the extracted parameters are obtained from the curve fitting of the homoepitaxial layers data as those that were given in the inserts of Figure 1b and 2a for the p-GaAs:Zn reference wafer.

Homoepitaxial layers	R = [TBAs]/[TMGa]	ΔE_{BGN} [eV]	Dopants density, P [$10^{18}\,cm^{-3}$]
GaAs#299	6	0.0331 ± 0.0028	2.1 ± 0.6
GaAs#304	8	0.0396 ± 0.0035	3.6 ± 1.0
GaAs#300	10	0.0332 ± 0.0023	2.1 ± 0.5
GaAs#301	12	0.0404 ± 0.0012	3.9 ± 0.4
GaAs#302	14	0.0352 ± 0.0021	2.5 ± 0.5

We can see on one hand that the BGN values are very similar and consequently are also the dopants density P and on the other hand that the dopant density is rather high. Moreover, we note that the R ratio has no significant influence on these extracted values, at least in this investigated range, as we do not observe any correlation between the R ratio (indicated close to the data points) and the dopants density or the bandgap narrowing. This conclusion will be evidenced more directly in the next paragraph focused more precisely on the presentation of the R ratio influence on the extracted parameters of the homoepitaxial layers.

4.2.2. Influence of the R Ratio on all the Extracted Parameters from the Fitting with Equation (4)

In **Figure 3**, we report the R influence on all the extracted parameters P, θ_p, p, and α from the fitting with Equation (4) to the bandgap variation with temperature of the homoepitaxial layers. Just for comparison, when relevant we have also reported the data points corresponding to the p(Zn)-GaAs reference wafer.

The data are also supplemented in **Table 3** along with the bandgap narrowing extracted from Equation (3) as explained in the preceding paragraph. Note that the numerical values of the three parameters θ_p, p, and α have just been indicated once because they are strictly identical whether they have been extracted from the fitting either with Equation (3) or (4), as explained at the end of Section 2.

We note no significant influence of the R ratio on the dopant concentration (Figure 3a), as already mentioned in the preceding paragraph, whereas a clear increase of the (near) average phonon temperature θ_p is observed in Figure 3b as the ratio R increases. We note also in Figure 3c,d that the uncertainties on the extracted parameters p and α are too high to observe any significant tendency on the R influence on these two last parameters. The explanation of this is related to the too restricted investigated temperature range at low and high temperatures where these two parameters contribute more to the bandgap variation. From Equation (1), indeed one can derive that the temperature-dependent term of $E_g(T)$ is mainly controlled by the linear term $(-\alpha T)$ when $T \gg \theta_p$ and by the T^p term when $T \ll \theta_p$. Taking into account a mean numerical value of θ_p around 250 K, as shown in Figure 3b, means that we need to go to a temperature lower (higher) than 20 K (600 K) in order to be highly sensitive to the parameter "p" (α), respectively. This shows the large temperature range around [20 K, 600 K] that is needed to be highly sensitive to all the parameters of the model. However, Figure 3a,b shows that with our investigated temperature range [80 K, 340 K], we can be sensitive enough to investigate the influence of growth parameters on the dopant density, which was our main goal in a first instance, and also that some additional information could be gained from the average phonon temperature θ_p evolution.

Even if the purpose of this article is focused on the characterization method, we can mention that the high doping concentration found whatever the R ratio may have two more probable origins: either it can be related to a high carbon content which is known to be a classical p-type dopant in GaAs, intentional or not,[11] or it can be related also to the GaAs antisite, an usual

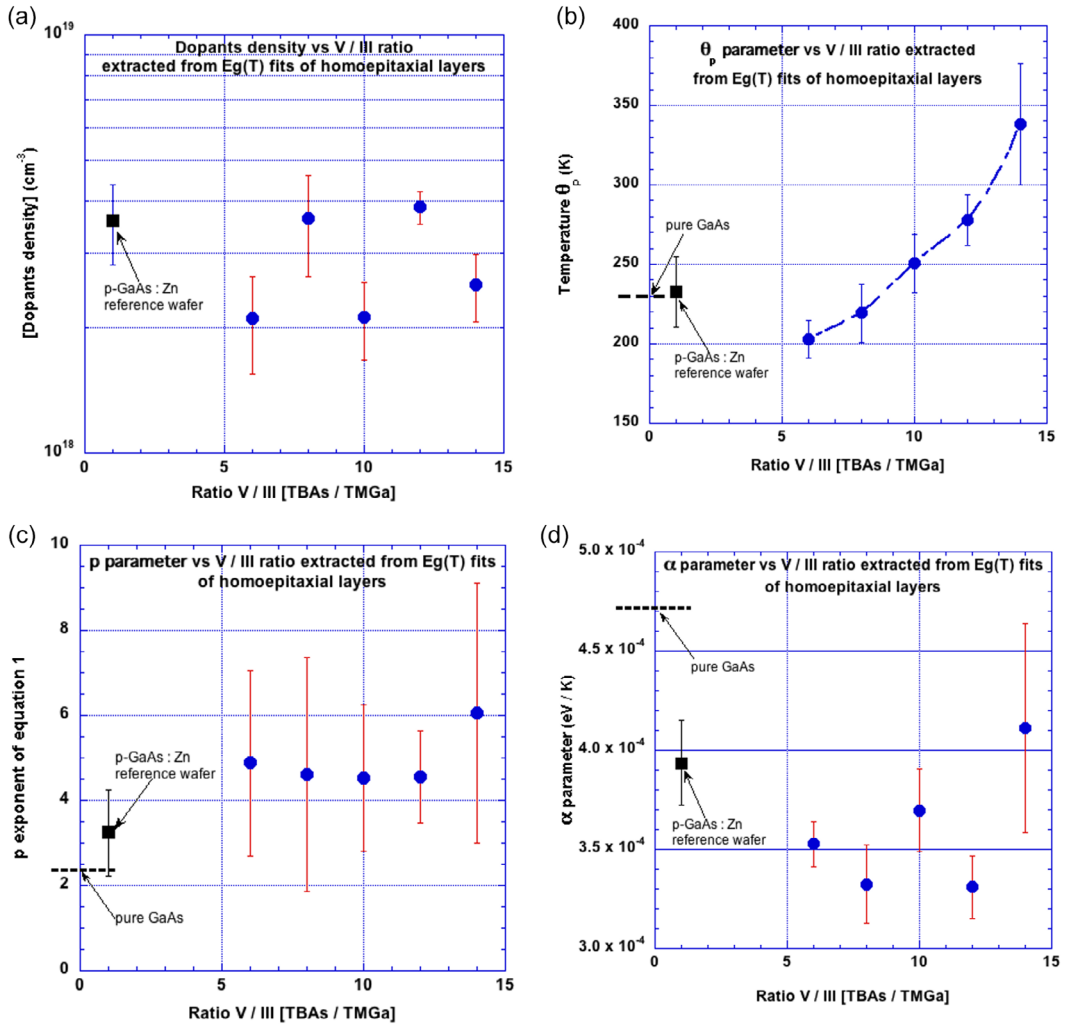

Figure 3. Influence of the V/III ratio (R) on the extracted parameters from the curve fitting with Equation (4) to the experimental bandgap variation with temperature of the GaAs homoepitaxial layers. The blue symbols are the experimental data and the blue dashed-dotted line is just a guide to the eye: a) doping density evolution with R, b) temperature θ_p evolution with R, c) p evolution with R, and d) α evolution with R. The error bars correspond to the uncertainties on the extracted parameters as those that were given in the inserts of Figure 1b and 2a. For comparison, we have also added the data for the p-GaAs:Zn reference wafer (black squared symbol arbitrarily located at $R = 1$).

Table 3. Extracted parameters P, θ_p, p, and α from the fitting with Equation (4) to the bandgap variation with temperature of the homoepitaxial layers grown with different $R =$ V/III ratio. For convenience, we have also repeated the numerical values of the bandgap narrowing already given in Table 2. The given uncertainties on the extracted parameters are obtained from the curve fitting of the homoepitaxial layers data as those that were given in the inserts of Figure 1b and 2a for the p-GaAs:Zn reference wafer. For comparison, are also given the numerical values of the extracted parameters corresponding to the two GaAs reference wafers.

Sample name	R	ΔE_{BGN} [meV]	Dopants density, P (10^{18} cm^{-3})	θ_p [K]	Exponent P	α [10^{-4} eV K^{-1}]
GaAs#299 homo-epi layer	6	33.1 ± 2.8	2.1 ± 0.6	203 ± 12	4.9 ± 2.2	3.53 ± 0.12
GaAs#304 homo-epi layer	8	39.6 ± 3.5	3.6 ± 1.0	219 ± 18	4.6 ± 2.8	3.32 ± 0.20
GaAs#300 homo-epi layer	10	33.2 ± 2.3	2.1 ± 0.5	251 ± 18	4.5 ± 1.7	3.70 ± 0.21
GaAs#301 homo-epi layer	12	40.4 ± 1.2	3.9 ± 0.4	278 ± 16	4.6 ± 1.1	3.31 ± 0.16
GaAs#302 homo-epi layer	14	35.2 ± 2.1	2.5 ± 0.5	338 ± 38	6.1 ± 3.1	4.11 ± 0.53
Semi-insulating GaAs reference wafer	–	4.5 ± 2.5	$(3.1 \pm 5.9) \times 10^{-3}$	217 ± 15	3.0 ± 0.6	4.68 ± 1.61
p-GaAs:Zn reference wafer	–	39.5 ± 2.8	3.6 ± 0.8	233 ± 22	3.2 ± 1.0	3.94 ± 0.21

intrinsic p-type defect in GaAs.[12] As we have shown in the past that a high carbon concentration was detected in our sample grown with the TMGa precursor,[3] here we have explored the R influence on the dopant concentration because Longo et al.[11] found that increasing the R ratio with TBAs flow rate increase can help to have a better decomposition of the Ga-$(CH_3)_3$ trimethyl gallium radicals which otherwise leads generally to incorporation of Ga-CH_3 gallium monomethyl radicals instead of gallium atoms incorporation only in the growing layer. The fact we have found here no effect of the R ratio on the dopant content could mean either that this ratio should be increased to much more higher values than the highest one investigated here or that the Ga_{As} antisite could be the predominant doping defect in our samples. Further work is in progress to analyze both hypothesis. In particular, we are also exploring the growth with the TEGa (triethylgallium) precursor instead of TMGa which is also an alternative to decrease the carbon incorporation.[13]

5. Conclusion

We have shown that the use of the PL technique associated with a modeling of the bandgap temperature dependence taking also into account the bandgap narrowing is an interesting noncontact technique to have a good order of magnitude of the dopant density in p-type GaAs material for concentration higher than 10^{16} cm^{-3}. We first assessed the method on two GaAs reference wafers spanning a large carrier density range from semi-insulating characteristics to highly p-doped ones. As an illustration, we then applied the technique to investigate the influence of the gas precursors flow rates ratio R = [TBAs]/[TMGa] on the residual doping in homoepitaxial layers grown with chemical beam epitaxy. In the relatively restricted R range from 6 to 14, we have not seen any influence on the residual doping density but a monotonous increase of the average phonon temperature was observed and correlated to the increase of the V/III ratio. Discussing its meaning is not the purpose of this article; however, this shows the ability and sensitivity of the technique to investigate the growth parameters influence with a cost-efficient contactless method.

Using this technique in the [80 K, 340 K] experimental temperature range leads to relative uncertainties comprised between 10% and 28% of the dopant density determination and between 5% and 11% of the average phonon temperature. This precision could be improved further with smaller temperature steps than the 20 K ones used in the present work and also extending the investigated temperature range if one needs a high sensitivity on all the modeling parameters.

The PL technique is well known for a long time to be very sensitive qualitatively to defects in semiconductors. However, as an optical technique, concerning the defects density, its quantitative sensitivity is also known to be lower than electrical methods such as capacitance measurements. However from the present work we can conclude finally that the PL technique is an interesting and convenient noncontact technique to extract the doping content of semiconductors without the need of a device fabrication. This optical spectroscopic technique can supplement standard electrical characterization techniques when these cannot be implemented easily due to too small object under test dimensions for instance.

Acknowledgements

This work was partly supported by the French National Research Agency, ANR (project HELLO-PV ANR22-CE050-0011).

Conflict of Interest

The authors declare no conflict of interest.

Data Availability Statement

The data that support the findings of this study are available from the corresponding author upon reasonable request.

Keywords

bandgap temperature dependence, doping extraction, modeling, photoluminescence

Received: July 31, 2024
Revised: November 18, 2024
Published online:

[1] D. Mencaraglia, C. Renard, J. P. Connolly, N. Cherkashin, G. Hallais, A. Jaffré, J. Alvarez, G. Chau, L. Vincent, J–P. Kleider, F. Hamouda, D. Bouchier, in *36th European Union Photovoltaic Solar Energy Conf. Proc. (EU PVSEC)*, WIP GmbH & Co Planungs-KG, Sylvensteinstr, München **2019**. ISBN : 3-936338-60-4. https://doi.org/10.4229/EUPVSEC20192019-3BV.2.49.
[2] C. Renard, T. Molière, N. Cherkashin, J. Alvarez, L. Vincent, A. Jaffré, G. Hallais, J. Connolly, D. Mencaraglia, D. Bouchier, *Sci. Rep.* **2016**, *6*, 25328.
[3] T. Molière, A. Jaffré, J. Alvarez, D. Mencaraglia, J. Connolly, L. Vincent, G. Hallais, D. Mangelinck, M. Descoins, D. Bouchier, C. Renard, *J. Appl. Phys.* **2017**, *121*, 035704.
[4] Y. P. Varshni, *Physica* **1967**, *34*, 149.
[5] R. Pässler, *Phys. Status Solidi B* **1999**, *216*, 975.
[6] E. Grilli, M. Guzzi, R. Zamboni, L. Pavesi, *Phys. Rev. B* **1992**, *45*, 1638.
[7] S. C. Jain, J. M. Mc Gregor, D. J. Roulston, *J. Appl. Phys.* **1990**, *68*, 3747.
[8] S. C. Jain, D. J. Roulston, *Solid-State Electron.* **1991**, *34*, 453.
[9] C. Renard, N. Cherkasin, A. Jaffre, L. Vincent, A. Michel, T. Molière, R. Hamouche, V. Yam, J. Alvarez, F. Fossard, D. Mencaraglia, D. Bouchier, *Appl. Phys. Lett.* **2013**, *102*, 191915.
[10] E. S. Tok, J. H. Neave, M. J. Ashwin, B. A. Joyce, T. S. Jones, *J. Appl. Phys.* **1998**, *83*, 4160.
[11] M. Longo, R. Magnanini, A. Parisini, L. Tarricone, A. Carbognani, C. Bocchi, E. Gombia, *J. Cryst. Growth* **2003**, *248*, 119.
[12] J.-Y. Huang, L. Shang, S.-F. Ma, B. Han, G.-D. Wei, Q.-M. Liu, X.-D. Hao, H.-S. Shan, B.-S. Xu, *Chin. Phys. B* **2020**, *29*, 010703.
[13] C. R. Abernathy, P. W. Wisk, D. A. Bohling, G. T. Muhr, *Appl. Phys. Lett.* **1992**, *60*, 2421.